Eur. Phys. J. A **3**, 335–349 (1998)

THE EUROPEAN PHYSICAL JOURNAL A

Identification of baryon resonances in central heavy-ion collisions at energies between 1 and 2 AGeV

FOPI Collaboration

M. Eskef[6,a], D. Pelte[6], G. Goebels[6], E. Häfele[6], N. Herrmann[4,6], M. Korolija[6,12], Y. Leifels[4,6], H. Merlitz[4,6], S. Mohren[6], M.R. Stockmeier[6], M. Trzaska[6], J.P. Alard[3], A. Andronic[1], R. Averbeck[4], Z. Basrak[12], N. Bastid[3], I. Belyaev[7], D. Best[4], A. Buta[1], R. Čaplar[12], N. Cindro[12], J.P. Coffin[10], P. Crochet[4,10], P. Dupieux[3], M. Dželalija[12], L. Fraysse[3], Z. Fodor[2], A. Genoux-Lubain[3], A. Gobbi[4], K.D. Hildenbrand[4], B. Hong[9], F. Jundt[10], J. Kecskemeti[2], M. Kirejczyk[4,11], R. Kotte[5], R. Kutsche[4], A. Lebedev[7], V. Manko[8], J. Mösner[5], D. Moisa[1], W. Neubert[5], M. Petrovici[1], C. Pinkenburg[4], C. Plettner[5], P. Pras[3], F. Rami[10], V. Ramillien[3], W. Reisdorf[4], J.L. Ritman[4], B. de Schauenburg[10], D. Schüll[4], Z. Seres[2], B. Sikora[11], V. Simion[1], K. Siwek-Wilczynska[11], V. Smolyankin[7], M.A. Vasiliev[8], P. Wagner[10], G.S. Wang[4], K. Wisniewski[4,11], D. Wohlfarth[5], A. Zhilin[7]

[1] National Institute for Physics and Nuclear Engineering, Bucharest, Romania
[2] Central Research Institute for Physics, Budapest, Hungary
[3] Laboratoire de Physique Corpusculaire, IN2P3/CNRS, and Université Blaise Pascal, Clermont-Ferrand, France
[4] Gesellschaft für Schwerionenforschung, Darmstadt, Germany
[5] Forschungszentrum Rossendorf, Dresden, Germany
[6] Physikalisches Institut der Universität Heidelberg, Heidelberg, Germany
[7] Institute for Theoretical and Experimental Physics, Moscow, Russia
[8] Kurchatov Institute, Moscow, Russia
[9] Korea University, Seoul, Korea
[10] Institut de Recherches Subatomiques, IN2P3/CNRS, and Université Louis Pasteur, Strasbourg, France
[11] Institute of Experimental Physics, Warsaw University, Poland
[12] Rudjer Boskovic Institute, Zagreb, Croatia

Received: 26 June 1998 / Revised version: 2 September 1998
Communicated by V. Metag

Abstract. The mass distributions of baryon resonances populated in near-central collisions of Au on Au and Ni on Ni are deduced by defolding the p_t spectra of charged pions by a method which does not depend on a specific resonance shape. In addition the mass distributions of resonances are obtained from the invariant masses of $(p, \pi^{\pm})$ pairs. With both methods the deduced mass distributions are shifted by an average value of -60 MeV/c^2 relative to the mass distribution of the free $\Delta(1232)$ resonance, the distributions descent almost exponentially towards mass values of 2000 MeV/c^2. The observed differences between (p, π^-) and (p, π^+) pairs indicate a contribution of isospin $I = 1/2$ resonances. The attempt to consistently describe the deduced mass distributions and the reconstructed kinetic energy spectra of the resonances leads to new insights about the freeze out conditions, i.e. to rather low temperatures and large expansion velocities.

PACS. 25.75.-q Relativistic heavy-ion collisions – 14.20.Gk Baryon resonances with S=0

1 Introduction

In central heavy ion collisions the number of mesons produced increases with bombarding energy. In the energy range between 1 and 2 AGeV, 8% to 22% of the available energy is dissipated into this channel which predominantly consists of pions [1,2]. The amount of dissipated energy also depends on system mass: In central Au + Au reactions at 1 AGeV it is 8%, but 15% in central Ni + Ni reactions at the same bombarding energy. The process responsible for meson production is believed to be predominantly the excitation of baryon resonances during the early compression phase of the collision. In the later expansion phase these resonances decay. The primordial decay yields a number of different mesons, mainly pions. Mesons with masses higher than the pion mass, e.g. η, ρ, may subsequently decay also into several pions. In total, the average mass of the excited baryon resonances and the

[a] *on leave of absence from:* Energy Research Group, University of Damascus, Syria

number of pions produced by their decay chains increase with bombarding energy. This mechanism is the basic process of pion production which is used in nuclear transport models to describe the dynamics of relativistic heavy ion collisions [3–11]. In a recent publication [11] it was shown that all resonances up to the $\Delta(1950)$ resonance have to be included to successfully reproduce the experimental pion data at energies between 1 and 2 AGeV.

The experimental confirmation that baryon resonances are excited in relativistic heavy ion collisions is rather scarce. The earliest indication came from the comparison by Brockmann et al. [12] of the pion and proton energy spectra observed in 1.8 AGeV Ar + KCl reactions. This comparison was later extended with the attempt to determine the $\Delta(1232)$ resonance mass and temperature [13]. Similar analyses of the pion energy spectra measured in 1 AGeV Au + Au collisions were published in [14]. At much higher energies, i.e. 13.7 AGeV, the fraction of nucleons excited to the $\Delta(1232)$ resonance was determined for Si + Al, Pb reactions [15]. In this study also the invariant mass distribution of the $\Delta(1232)$ resonance was reconstructed from correlated (p, π^+) pairs.

To identify structures in the invariant mass distribution of correlated proton and pion pairs provides the direct proof that nucleons are excited to high-lying resonances. The major obstacle in reconstructing the invariant mass is the large background of non-correlated (p, π) pairs, which increases with the number of protons and is therefore particularly large for central reactions of heavy-mass systems. In peripheral reactions with very light projectiles, e.g. p [16,17] or ^{3}He [18] induced reactions at around 2 GeV bombarding energy, the (p, π^+) correlations were successfully analyzed and the mass distribution of the $\Delta(1232)$ resonance was determined. The resonance mass was found to be shifted by -25 MeV/c^2 to lower masses in reactions on various targets, compared to those on protons. Very recently the $\Delta(1232)$ was reconstructed from (p, π^+) pairs detected at 1.97 AGeV bombarding energy in ^{58}Ni + Cu collisions [19]. In this case much larger mass shifts of -75 MeV/c^2 were observed in central collisions, the shift became smaller with increasing impact parameter. That the $(p, \pi^\pm)$ pairs can also be successfully studied in central collisions of very heavy systems at 1 AGeV bombarding energy was shown in [20]. This report contained a preliminary analysis of the data used in the present publication. Although at 1 AGeV energy the excitation of the $\Delta(1232)$ resonance is the dominating channel there is direct experimental evidence from the identification of the η meson [21], that at this energy also higher-lying resonances, in particular the $N(1535)$ resonance, must become excited. If this is the case then the resonance decay into the 2π channel also has to be present, and the analysis of $(p, \pi^\pm)$ correlations will not yield a complete picture of the resonance distribution. On the other hand, the 2π decay channel can be observed in the pion transverse momentum spectra [11].

The subsequent sections are organized as follows: Sect. 2 contains a short description of the experimental procedures. A more detailed description can be found in [1]. The methods to extract the invariant mass distributions of the resonances involved are presented in Sect. 3. These methods include the analyses of the measured π^- and π^+ transverse momentum spectra, and the analyses of the (p, π^-) and (p, π^+) correlations. In both cases the residual Coulomb interaction between the charged pions and the positively charged baryon distribution causes a perturbation [1,2], which is of opposite sign for π^- and π^+ and which we compensate by analyzing the average of the π^- and π^+ spectra, respectively by taking the average invariant mass distribution from (p, π^-) and (p, π^+). The justification to apply this procedure is given in the Appendix 6.1. The experimental results are presented in Sect. 4, Sect. 5 contains their discussion and the summary.

2 Experimental procedures

The reactions ^{197}Au + ^{197}Au and ^{58}Ni + ^{58}Ni were studied at nominal beam energies of 1.06, respectively 1.06, 1.45 and 1.93 AGeV. The ^{197}Au and ^{58}Ni beams were accelerated by the $UNILAC/SIS$ accelerator combination of the GSI /Darmstadt. The duty cycle was 75% with a spill length of 4 s. The average beam intensities varied between $1 \cdot 10^5$ and $5 \cdot 10^5$ particles per spill. The targets consisted of self supporting foils with a thickness of 100μm(Au), respectively 270μm(Ni). This corresponds to an interaction probability of 0.5%. The energy loss of the beams in the targets is of around 0.01 AGeV and was neglected.

The particles produced by the Au + Au and Ni + Ni reactions were detected by the $FOPI$ detector which is a modular detection system with almost 4π coverage. Of particular importance for the present investigation is the central drift chamber CDC which is mounted inside the superconducting magnet with a solenoidal field of 0.6 T strength. The CDC has complete cylindrical symmetry, it covers the polar angles ϑ from 32° to 150° in the laboratory frame and allows the particles masses and charges to be simultaneously determined. For charged pions the geometrical boundaries of the CDC guarantees a detection efficiency of better than 65%, in particular the midrapidity region $|Y^{(0)}| < 0.1$ is fully covered above a transverse momentum limit $p_t^{(0)} > 0.65$ (for the definition of the variables used here, see below). Notice, however, that to distinguish the π^+ from protons an additional momentum limit $p < 0.65$ GeV/c was introduced [1]. This limit which corresponds to $p_t^{(0)} = 3.2$ at midrapidity, has no consequences for the situation shown in Fig. 1, and it is not required for the π^-. For protons the geometrical CDC boundaries $32° < \vartheta < 150°$ reduce their detection efficiency to approximately 45%.

The situation for particles produced in symmetric reactions at 1.93 AGeV bombarding energy is depicted in Fig. 1. The fully drawn curves display the lower and upper geometrical limits $\vartheta_l = 32°$ and $\vartheta_u = 150°$ in the laboratory frame, the dotted curves are drawn for pions respectively protons with cm kinetic energies of 300 MeV. The shaded area displays the momentum distribution of identified $\Delta(1232)$ resonances, i.e. the decay proton and pion

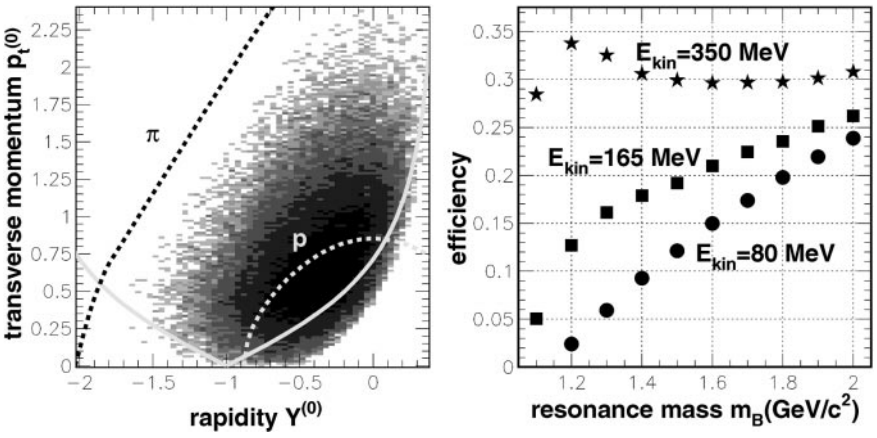

Fig. 1. Left panel: The reconstructed momentum distribution of thermal $\Delta(1232)$ resonances with a temperature of 173 MeV. The full curves display the geometrical limits of the CDC, the dashed curves display the momenta of pions, respectively protons with a kinetic energy of 300 MeV. Right panel: The efficiency of reconstructing resonances with masses $m_{\rm B}$ and with kinetic energies $E_{\rm kin}$ from (p,π) pairs detected by the CDC

were measured by the CDC. The resonances are Monte Carlo generated using a fixed mass $m_\Delta = 1232$ MeV/c^2 and an isotropic Boltzmann distribution with temperature $T = 173$ MeV, which corresponds to a mean kinetic energy of 300 MeV. Because of the decay into a correlated (p,π) pair the $\Delta(1232)$ resonance can be observed in regions of the momentum space which are prohibited for single pions or protons by the $\vartheta_{\rm l} = 32^\circ$ cut. At midrapidity the $\Delta(1232)$ resonance is detected for transverse momenta $p_{\rm t}^{(0)} > 0.5$. Notice that the symmetry law

$$f(\Theta,\Phi) = f(\pi-\Theta,\pi+\Phi) \ , \qquad (1)$$

which holds for all symmetric reactions guarantees that the region $Y^{(0)} > 0$ can be reconstructed by reflection around midrapidity from the region $Y^{(0)} < 0$. In this way the properties of around 50% af all $\Delta(1232)$ resonances are known. The remaining ones which cannot be reconstructed decay into a (p,π) pair, where either one of the two particles or both are not detected within the geometrical boundaries of the CDC. Under the assumptions made, i.e. isotropic resonance distribution and isotropic resonance decay, the efficiency of the CDC for detecting resonances can be calculated as a function of the mass and the kinetic energy of the resonance. The efficiencies to detect resonances with masses $m_{\rm B}$ and kinetic energies $E_{\rm kin}$ are plotted in the right panel of Fig. 1, without employing symmetrization. The detection efficiencies decrease rapidly with mass for small kinetic energies. Without the proper efficiency corrections, which in this case are solely due to the incomplete 4π acceptance of the detector, the contributions from small mass values $m_{\rm B}$ would be reduced. Notice that from the results published in [22] for the Au + Au reaction at 1 AGeV bombarding energy, the expected mean kinetic energy of the $\Delta(1232)$ resonance with mass $m_\Delta = 1232$ MeV/c^2 is $< E_{\rm kin} >= 200$ MeV. To obtain the efficiency correction for a given mass the data shown in Fig. 1 have to be weighted by the energy distribution of that mass and integrated.

In addition to the CDC, the information from the forward plastic scintillation wall PLA mainly served trigger purposes. The PLA is a high-granularity component of the $FOPI$ detector and covers the polar angles ϑ from 7° to 30° with full cylindrical symmetry. It separates particles only according to their charges. In the present analysis the particle multiplicities $n_{\rm PLA}$ measured with the PLA were required to be larger than 80% of the maximum multiplicity which is defined by the lower boundary of the $PM5$ multiplicity bin, see [1,2]. This multiplicity criterion selects near-central collisions in the impact parameter range from 0 to $0.3\,b_{\rm max}$, where $b_{\rm max}$ is the maximum impact parameter of a given reaction. On the average the fireball then contains around 3/4 of the maximum number $A_0 = A_{\rm proj} + A_{\rm targ}$ of nucleons.

In the present study we shall use the identical conventions which were used in [1,2]. All quantities which refer to the laboratory(lab) or target frames will be labeled by small letters. The center of mass(cm) or fireball frames are generally characterized by capital letters. Exceptions are those quantities, like the transverse momentum, which remain unchanged under the transformation of frames. For the transverse momentum we sometimes use the quantity $p_{\rm t}^{(0)}$ where the index $^{(0)}$ indicates a normalization by the factor $(A \cdot P_{\rm proj}/A_{\rm proj})^{-1}$ and where A is the particle's mass number. Similarly the rapidity Y in the cm frame is normalized by the factor $(Y_{\rm proj})^{-1}$ and this quantity is labeled $Y^{(0)}$. In the present experiments the normalization factors for the pion transverse momenta have the values $9.47, 8.09, 7.02$ (GeV/c)$^{-1}$ for $1.06, 1.45, 1.93$ AGeV bombarding energy, to obtain the equivalent values for protons these numbers should be multiplied with a factor 0.149. For the rapidities the corresponding normalization factors are $1.44, 1.26, 1.12$.

The data from the drift chamber CDC were analyzed by using three different tracking algorithms as described in [1]. Differences in tracking are mainly observed in case of the Au + Au reaction, they consist in a slightly different (10%) efficiency with which negative pions are identified. Equal tracking efficiencies can be obtained by adjusting the limits in which the tracking parameters are allowed to vary [1]. We have verified that our results do not depend on these limits, and agree for the different versions of the tracking algorithm. Our final data, i.e. transverse momentum and invariant mass spectra, are the average of three independent analyses with these different trackers, and this data sample has been used before in our study of the pion production in Au + Au [1] and Ni + Ni [2]

reactions. The accuracy with which the particle momenta can be measured with the CDC was determined in [1]. For the transverse momentum the relative standard deviation $\sigma(p_t)/p_t$ is 0.04 for $p_t < 0.5$ GeV/c, and then increases to 0.1 for transverse momenta $p_t = 1.5$ GeV/c. The accuracy in determining the azimuthal angle φ is better than 1°, the accuracy to determine the polar angle ϑ is better for protons ($\sigma(\vartheta) = 3°$) than for pions ($\sigma(\vartheta) = 5°$). These values may be used to estimate the accuracy with which the mass m_B of a baryon resonance B can be determined. Without going into the details which will be more fully presented in the next section, the accuracy estimate is

$$\frac{\sigma(m_B)}{m_B} = \frac{m_B^2 - m_0^2}{m_B^2} \times 0.5\sqrt{\left(\frac{\sigma(p_p)}{p_p}\right)^2 + \left(\frac{\sigma(p_\pi)}{p_\pi}\right)^2 + (\sigma(\alpha)\tan\alpha)^2} \quad , \quad (2)$$

where m_0 is the sum of the proton and pion masses and α is the angle between $\mathbf{p}_p$ and $\mathbf{p}_\pi$. Taking representative values, i.e.

$$\frac{\sigma(p_p)}{p_p} = 0.06 \quad , \quad \frac{\sigma(p_\pi)}{p_\pi} = 0.04 \quad , \quad \sigma(\alpha)\tan\alpha = 0.09$$

one obtains for, e.g. the mass of the $\Delta(1232)$ resonance an error of $\sigma(m_\Delta) = 20$ MeV/c^2, with decreasing accuracy for larger masses m_B. This estimate is certainly sufficient to determine the resonance mass distribution, it is however not representative, since a second source of systematic errors comes from the reconstruction of the combinatorial background of uncorrelated $(p, \pi^\pm)$ pairs, as will be discussed in the next section. In the present analysis the number of directly measured $(p, \pi^\pm)$ pairs is larger than 10^6 for a given reaction, to reconstruct the background for this reaction we have used approximately 10 times more pairs. The statistical errors are therefore not the decisive factor in our analysis.

3 Methods of analysis

We have employed two independent procedures to determine the mass distribution of baryon resonances excited in near-central collisions of identical nuclei. In the first method the pion p_t spectrum is defolded to yield the mass distribution, in the second method the invariant mass distribution of the correlated $(p, \pi^\pm)$ pairs is deduced from the data. Both methods rely on the assumption that the resonances involved in the production of pions decay via the emission of only one pion. This assumption is not necessarily fulfilled as was pointed out in the introduction. If the two-pion decay is present it effects the results of the two methods in different ways. In the first case the presence of the two-pion channel will cause a distortion of the mass spectrum, in the second case it will mainly contribute to the background. It is therefore not expected that both methods should yield identical results, however these results should be reasonably close since the two-pion channel is expected to be weak [11]. We therefore also take a reasonable agreement as an indication that systematic errors are sufficiently small.

3.1 The analysis of the p_t spectra

The defolding of the experimental p_t spectra of charged pions was the earliest method applied by Brockmann et al. [12,13] to deduce the mass of the $\Delta(1232)$ resonance. Recently this technique was also applied by [23] to defold the p_t distribution of π^+ from Au + Au reactions. It is well known that the p_t spectrum of π^+ differs from the p_t spectrum of π^- for momenta $p_t < 0.3$ GeV/c, and that this difference is caused by the Coulomb interaction between the pions and the nuclear matter distribution [1, 2]. In the Appendix 6.1 we shall explore this effect more closely and show that the Coulomb effects cancel when the p_t spectra of π^+ and π^- are combined. We follow this prescription in our analysis and add the p_t spectra of π^- and π^+, measured in a narrow rapidity gap $|Y^{(0)}| < 0.1$. The individual p_t spectra of π^- and π^+ have almost identical cross sections for $p_t > 0.3$ GeV/c [2], this part of the p_t spectra thus supplied the required normalization factor. The pion p_t spectrum is defolded under the hypothesis that it is entirely due to the one-pion decay of excited baryon resonances:

$$\frac{d\sigma_j}{dp_t} = \sum_{i=1}^{n} \frac{d\sigma_{ij}(T,\beta)}{dp_t} \cdot f(m_i) \quad ; \quad max(j) \geq n \ , \quad (3)$$

where $d\sigma_{ij}/dp_t$ is the midrapidity transverse momentum distribution of pions which are emitted in the decay of a baryon resonance with mass $m_i > m_0$. In [24] the method is described to calculate $d\sigma_{ij}/dp_t$. This distribution depends only weakly on the kinetic energy distribution of the resonances, a phenomenon which was first noticed by Brockmann et al. [12,13]. Using the formula of Siemens and Rasmussen [25] the kinetic energy distribution is usually parametrized by the nuclear temperature T and the flow velocity β. For these we have used in our analysis the values published in [22] for the Au + Au, and in [26] for the Ni + Ni systems. These values of T and β are listed in Table 1. The defolding of (3) was performed with the EM algorithm [27]. The EM algorithm finds after a sufficient number of iterations the Maximum-Likelihood estimate of $f(m_i)$. Its performance and accuracy, particularly when applied to defolding the pion p_t spectra, was studied in detail in [28]. It was shown that the result is unambiguous and independent of the initial $f(m_i)$ distribution, when the functions $d\sigma_{ij}(T,\beta)/dp_t$ are linear independent. The mass resolution obtained by the defolding was studied as a function of the number of iterations by means of the point-spread-functions of m_i. Allowing for infinite number of iterations the mass resolution reaches for all m_i its ideal value of 10 MeV/c^2 in accordance with the width of the used mass bins. Limiting the number of iterations the mass resolution decreases especially for larger masses. The number of iterations is, however, bounded by

Table 1. Temperatures T and flow velocities β used in defolding the measured p_t spectra of $\pi^{\pm}$. The $r^{\pm}$ and $r_e^{\pm}$ values give the measured, respectively calculated (6) fraction of correlated (p,π^+) respectively (p,π^-) pairs, $\kappa_p^{\pm}$ is the probability that the proton escapes unscattered. The first row is for the Au + Au reaction, the next three rows for the Ni + Ni reactions

energy (AGeV)	T (MeV)	β	r^+ (%)	r_e^+ (%)	κ_p^+	r^- (%)	r_e^- (%)	κ_p^-
1.06	81	0.32	0.75 ± 0.25	0.75	1.0 ± 0.3	0.6 ± 0.2	0.22	2.7 ± 0.9
1.06	79	0.23	1.0 ± 0.3	2.17	0.46 ± 0.15	0.75 ± 0.25	0.68	1.1 ± 0.35
1.45	84	0.29	0.95 ± 0.3	2.16	0.44 ± 0.15	0.6 ± 0.2	0.71	0.85 ± 0.3
1.93	92	0.32	1.05 ± 0.3	2.19	0.48 ± 0.15	0.6 ± 0.2	0.71	0.85 ± 0.3

the statistical errors of the measured $d\sigma_j/dp_t$ spectrum. The iterations are stopped when the calculated spectrum (right hand side of (3)) becomes identical with the measured $d\sigma_j/dp_t$ spectrum within these errors. Otherwise the algorithm would run into describing the statistical fluctuations. The mass resolution reached for masses in the important region $m_i < 1400$ MeV/c^2 was $10 - 30$ MeV/c^2, for masses $m_i < 1700$ MeV/c^2 it still remained below 50 MeV/c^2. These errors are the statistical uncertainties for a mass bin m_i, the accuracy to determine the mean value of the mass distribution $f(m_i)$ is much better and in fact mainly determined by systematic errors which we have deduced from a comparison between our two different techniques to obtain $f(m_i)$.

3.2 The analysis of the $(p,\pi^{\pm})$ pairs

The invariant mass of a $(p,\pi^{\pm})$ pair can in principle be calculated from the measured momenta $\mathbf{p}_p$ and $\mathbf{p}_\pi$ via

$$m_B = \sqrt{(e_p + e_\pi)^2 - (\mathbf{p}_p + \mathbf{p}_\pi)^2} \quad \text{where} \tag{4}$$

$$e_p = \sqrt{(p_p)^2 + (m_p)^2} \quad \text{and} \quad e_\pi = \sqrt{(p_\pi)^2 + (m_\pi)^2}.$$

For many of such pairs the resulting mass distribution $dn^{\pm}_{(meas)}/dm_B$ contains a large combinatorial background contribution $dn^{\pm}_{(back)}/dm_B$ from uncorrelated $(p,\pi^{\pm})$ pairs, which has to be subtracted from the former in order to obtain the required mass distribution $dn^{\pm}/dm_B$ of truly correlated pairs:

$$\frac{dn^{\pm}}{dm_B} = \frac{dn^{\pm}_{(meas)}}{dm_B} - \left(1 - r^{\pm}\right) \frac{dn^{\pm}_{(back)}}{dm_B} \quad . \tag{5}$$

In this expression $dn^{\pm}_{(meas)}/dm_B$ and $dn^{\pm}_{(back)}/dm_B$ are normalized to equal intensity, and $r^{\pm}$ is the ratio of the number of "true" pairs to the number of "random" pairs. It is assumed that $r^{\pm}$ is constant, i.e. does not depend itself on m_B, which follows from the condition that $dn^{\pm}_{(back)}/dm_B$ is correctly known. The analysis consists of determining the size of $r^{\pm}$ and the shape of the background contribution $dn^{\pm}_{(back)}/dm_B$.

The generally accepted way to obtain the background spectrum is based on the method of event mixing. This method takes the proton and the pion of a pair not from the same event but from different events, using the fact that all "true" correlations do not exist in mixed pairs, but that "random" correlations will survive the mixing. Besides the true correlations due to the resonance decay there are additional correlations due to the reaction dynamics as, for example, the particle focussing with respect to the event plane. These latter correlations are also destroyed by event mixing and therefore are not removed when subtracting the mixed spectrum from the measured spectrum unless special precautions are taken. These require that for the pairs measured in a certain event the corresponding mixed pairs come from events with identical proton and pion multiplicities and identical orientation of the event plane. The latter requirement can always be fulfilled by the proper rotation of both events around the beam axis. The condition of equal multiplicities in the measured and mixed spectra also ensures that correlations due to pion rescattering in spectator matter [1,2] are properly subtracted.

The general question of how reliably the uncorrelated background spectrum can be reconstructed by means of the event mixing technique was studied in detail by L'Hote [29]. In the majority of cases the difference between the measured and mixed spectrum (right hand side of (5)) includes, besides the invariant mass distribution from true pairs, a residual contribution from random pairs which becomes the smaller, the smaller the differences between the phase space distributions of protons and baryon resonances. We have confirmed these conclusions with our Monte Carlo studies, and have found that in the present case, where the decay is dominated by the $\Delta(1232)$ resonance and where the temperatures T are moderate, the contribution of random pairs to the right hand side of (5) is small. In addition we take the agreement with the results from the defolding procedure as independent evidence that the event mixing technique is reliable in the present analysis.

With the method at hand to determine $dn^{\pm}_{(back)}/dm_B$ it is easy to prove that the measured $dn^{\pm}_{(meas)}/dm_B$ spectrum contains a contribution from correlated $(p,\pi^{\pm})$ pairs. For this purpose we assume $r^{\pm} = 0$ and calculate $dn^{\pm}/dm_B$ according to (5). The resulting spectrum has total intensity zero, the correlations appear as regions of positive respectively negative intensities for certain values of m_B. This is shown in Fig. 2 for the Au + Au reaction at 1.06 AGeV bombarding energy. The correlation signals are strikingly strong and they provide the undisputable

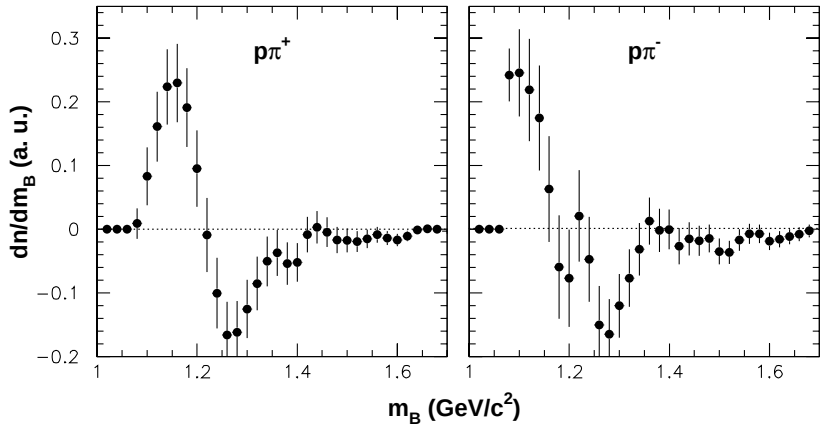

Fig. 2. The signal for the existence of correlated (p, π^+) (left panel), respectively (p, π^-) pairs (right panel) in the reaction Au + Au at 1.06 AGeV bombarding energy. The total intensity in the correlation spectra is normalized to zero

evidence that part of the $(p, \pi^{\pm})$ pairs are correlated due to the decay of baryon resonances.

In order to extract the mass distribution of these resonances the ratios $r^{\pm}$ have to be experimentally determined. The determination is done in principle, i.e. when statistical fluctuations are negligible, by the requirement that the right hand side of (5) should be positive. In reality these fluctuations cause part of the $dn^{\pm}/dm_{\rm B}$ spectrum to attain negative values. From Monte Carlo calculations with similar counting statistics as in the experiments we have concluded that the negative part may vary between 2% and 5% of the total positive intensity. These fractions provided the proper criteria for the background subtraction and the determination of the $r^{\pm}$ values within an uncertainty of 30%. Furthermore, the resulting $dn^{\pm}/dm_{\rm B}$ distribution depends only weakly on the chosen value of $r^{\pm}$ in the region where $dn^{\pm}/dm_{\rm B}$ has its maximum. The values obtained for r^+ respectively r^- are listed in Table 1.

The relative contribution of correlated pairs $r^{\pm}$ can be calculated from the measured proton multiplicity $n_{\rm p}$ and the known detection efficiency for protons $\epsilon_{\rm p}$:

$$r^{\pm} = \frac{\epsilon_{\rm p}}{n_{\rm p}} \alpha_{\rm I}^{\pm} \kappa_{\rm p}^{\pm} \xi_{\pi} \quad , \tag{6}$$

where $\alpha_{\rm I}^{\pm}$ is an isospin dependent factor which takes into account that part of the detected pions are correlated with undetected neutrons, $\kappa_{\rm p}^{\pm}$ is the probability that the proton reaches the detector without another proton - nucleon interaction, and ξ_{π} describes the fraction of the pions which are correlated, i.e. due to resonance decay. The factor $\alpha_{\rm I}^{\pm}$ depends on the isospin of the decaying resonance and is different for π^- and π^+. For isospin $I = 1/2$ one obtains $\alpha_{1/2}^- = 1$ and $\alpha_{1/2}^+ = 0$ for π^- and π^+, respectively, for $I = 3/2$ the corresponding factors are $\alpha_{3/2}^- = (N + 2 \cdot Z)/(10 \cdot N + 2 \cdot Z)$ and $\alpha_{3/2}^+ = 9 \cdot Z/(10 \cdot Z + 2 \cdot N)$. Notice that $I = 1/2$ resonances cannot be observed in the (p, π^+) channel. The isospin factors for $I = 3/2$ resonances depend on the N over Z ratio. For the Au + Au reaction one obtains $\alpha_{3/2}^+ = 0.69, \alpha_{3/2}^- = 0.21$, for the Ni + Ni reactions these factors are $\alpha_{3/2}^+ = 0.74, \alpha_{3/2}^- = 0.24$. Assuming a negligible contribution from thermal pions ($\xi_{\pi} = 1$) and that only the decay of $I = 3/2$ resonances contribute to the yield of correlated pairs ($\alpha_{\rm I}^{\pm} = \alpha_{3/2}^{\pm}$), (6) provides an upper limit $r_{\rm e}^{\pm}$ of $r^{\pm}$ when $\kappa_{\rm p}^{\pm} = 1$. The values of $r_{\rm e}^{\pm}$ are quoted in Table 1. The direct comparison between $r^{\pm}$ and $r_{\rm e}^{\pm}$ gives the experimental values of $\kappa_{\rm p}^{\pm}$ also quoted in Table 1. The errors of $\kappa_{\rm p}^{\pm}$ orginate from the uncertainty of $r^{\pm}$ (30%). In the next Section we shall discuss the consequences which follow from these $\kappa_{\rm p}^{\pm}$ values.

4 Experimental results

4.1 Results from the $p_{\rm t}$ distributions

The pion $p_{\rm t}$ spectra obtained by adding the measured π^+ and π^- spectra in the rapidity range $-0.1 \leq Y^{(0)} \leq 0.1$, are displayed in Fig. 3. For the defolding by means of the method presented in Sect. 3.1 we have used the temperatures T and the radial flow velocities β determined by [22] and [26] and listed in Table 1. The mass distributions are shown as histograms in Fig. 4. The shaded areas represent the uncertainties of the defolding technique. These uncertainties are firstly due to the possible changes in the values of T and β, and secondly due to the possible contribution of the 2π decay channel to the low-momentum part of Fig. 3. Considering the first point first it should be mentioned that a recent analysis [30] of the reaction Au + Au at 1.06 AGeV incident energy indicates a lower value of the temperature ($T \approx 50$ MeV) and a larger value for the collective velocity ($\beta \approx 0.5$) yielding a 10% larger mean kinetic energy of the $\Delta(1232)$ resonance than deduced from Table 1. In order to estimate the changes which may result from different values of the temperature and the flow we have repeated the defolding of all pion $p_{\rm t}$ spectra using a 40% smaller value of T and values of β which correspond to a 10% increase in mean kinetic energy. The uncertainties of $f(m_{\rm i})$ are given by the shaded areas in Fig. 4. The uncertainty contributions from the decay into two pions were estimated by starting the defolding of the $p_{\rm t}$ spectra first at momentum values $p_{\rm t} = 0.1$ GeV/c and then at $p_{\rm t} = 0.15$ GeV/c. Also these changes are included in the shaded areas in Fig. 4.

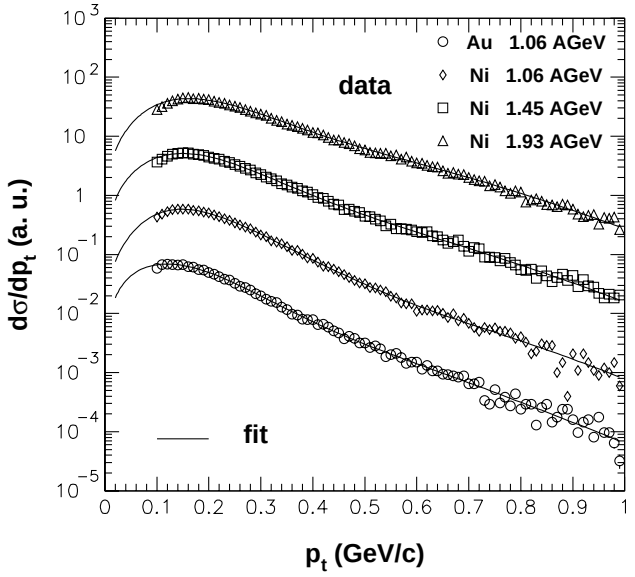

Fig. 3. The measured (open symbols) and calculated (full curves) transverse momentum spectra in the rapidity range $|Y^{(0)}| < 0.1$ for the reactions Au + Au (Au) and Ni + Ni (Ni) at the stated incident energies

The main features of the mass distributions obtained by the defolding technique are their shifts of approximately -60 MeV/c^2 away from the mass of the free $\Delta(1232)$ resonance, shown by the arrows in Fig. 4, and their weak extensions towards larger masses. These tails of the mass distributions are observed for all reactions, but it appears to be strongest in case of the Ni + Ni reaction at 1.93 AGeV bombarding energy.

4.2 Results from the $(p, \pi^{\pm})$ pairs

We first consider the effects which the residual Coulomb interaction between charged pions and the nuclear matter distribution might exert onto the reconstruction of invariant masses. In Fig. 5 the invariant mass distributions obtained from (p, π^+) respectively (p, π^-) pairs are shown for all reactions. These distributions are normalized to equal integrated intensity to allow for an easy comparison between the π^+ and π^- data. The values of $r^{\pm}$ deduced from this analysis and the corresponding values of $\kappa_{\rm p}^{\pm}$ are listed in Table 1. In all reactions the values of $\kappa_{\rm p}^-$ are larger than those of $\kappa_{\rm p}^+$. This is the behaviour one would expect if the resonance mass distribution contains an $I = 1/2$ component with a mean free mass above the $\Delta(1232)$ mass. The large value of $\kappa_{\rm p}^-$ in case of the Au + Au reaction, c.f. Table 1, requires a 25% contribution of $I = 1/2$ resonances to reduce it to its regular size of $\kappa_{\rm p}^- = \kappa_{\rm p}^+ \approx 1$. In case of the Ni + Ni reactions the $\kappa_{\rm p}^{\pm}$ are of size ≈ 0.6 with a 20% contribution of $I = 1/2$ resonances. These apparent differences between the Au + Au and Ni + Ni reactions are not understood yet. On the other hand, in all reactions the maxima of the mass distributions shown in Fig. 5 are shifted towards masses below the $\Delta(1232)$ mass. In order to quantify these results without taking resort to the Lorentz shape of a free resonance, we have calculated the mean mass $m_\Delta = < m_{\rm B} >$ and the standard deviation $\sigma_\Delta = \sqrt{< m_{\rm B}^2 > - < m_{\rm B} >^2}$ in the region of the prominent peak with an upper limit $m_{\rm B} < m_<$. For $m_<$ we have chosen a value $m_< = 1300$ MeV/c^2 which is motivated by a recent theoretical calculation of the $\Delta(1232)$ mass shape [31] and which shall be further discussed in the next section, c.f. Fig. 8. The results for m_Δ and σ_Δ are quoted in the first two rows of each reaction entry in Table 2. One notices that m_Δ from (p, π^+) pairs is on the average slightly larger than from (p, π^-) pairs, and that the opposite holds for σ_Δ. We interpret the first result as caused by the differences in the Coulomb interactions between π^+ respectively π^- and the baryons, whereas the second result again indicates the existence of $I = 1/2$ contributions which can only be present in the (p, π^-) channel.

The influence of the Coulomb interaction is studied in more detail in the Appendix 6.1, where it is shown that similar to the prescription employed in case of the defolding method, also in case of the $(p, \pi^{\pm})$ correlations the influence can be minimized by adding the invariant mass spectra of (p, π^+) and (p, π^-) pairs to yield the mass spectrum of $(p, \pi^{\pm})$ pairs. On the latter spectrum we will base our further analysis.

The mass spectra from $(p, \pi^{\pm})$ pairs are shown, together with the corresponding spectra from the defolding method, as points in Fig. 4. For each reaction these mass spectra obtained by two different techniques are very similar in the range around the prominent $\Delta(1232)$ peak. Notice that the efficiency corrections represented by Fig. 1 were not applied to the $(p, \pi^{\pm})$ data, but other corrections discussed in the Appendix 6.2 were applied. The reason that the influence of the detector geometry onto the invariant mass does not need to be considered is due to our finding from Monte Carlo simulations, that the corresponding decrease in the acceptance of small masses is counterbalanced by an enhancement caused by the finite detector resolution, see the Appendix. Both effects are of similar size and therefore cancel within the achieved experimental accuracies.

4.3 The $\Delta(1232)$ mass shift and higher-lying resonances

For a detailed analysis of the results presented in Fig. 4 we have applied the same methods used in the analysis of Fig. 5. The mean mass m_Δ and the standard deviation σ_Δ were deduced in the region $m_0 < m_{\rm B} < m_<$, their values are quoted in the last two rows of each reaction entry in Table 2. The mass shift of $\Delta m_{\rm B} = -71 \pm 6$ MeV/c^2 found for the Au + Au reaction appears to be significantly larger than the shifts found for the Ni + Ni reactions, which do not seem to depend on incident energy and which amount to $\Delta m_{\rm B} = -49 \pm 4$ MeV/c^2. The interpretation of these shifts is postponed to Sect. 5.

Finally the Fig. 4 illustrates that the measured mass distributions extend with weak tails to masses above $m_{\rm B} > m_<$. Only the $(p, \pi^{\pm})$ data prove that these tails

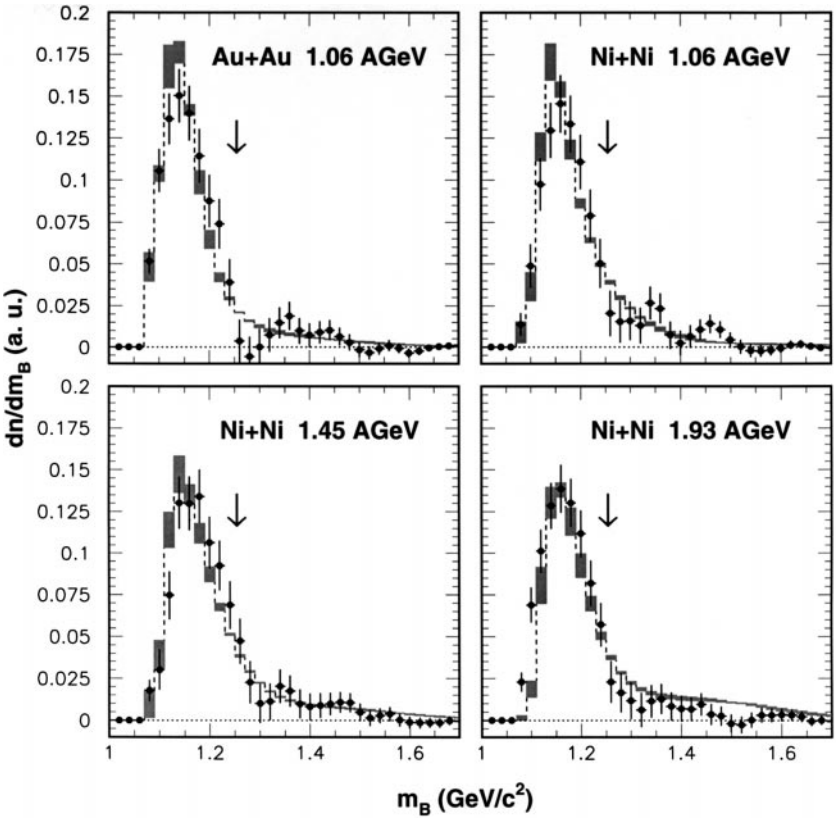

Fig. 4. The invariant mass spectrum of baryon resonances excited by the reactions stated in each picture. The shaded areas correspond to the analysis of the measured transverse momentum spectra of $\pi^{\pm}$, the full points to the analysis of the measured $(p, \pi^{\pm})$ pairs. The arrows point to the maximum of the free $\Delta(1232)$ mass distribution

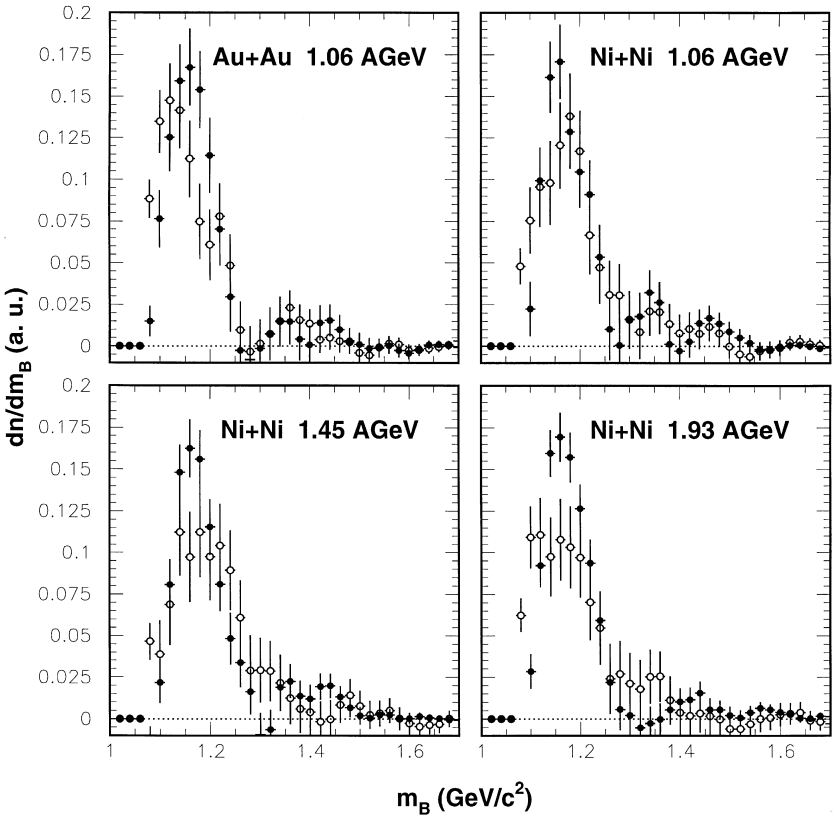

Fig. 5. The invariant mass spectra of correlated (p, π^{-}) (open points) and (p, π^{+}) (full points) pairs for the reactions stated in each picture

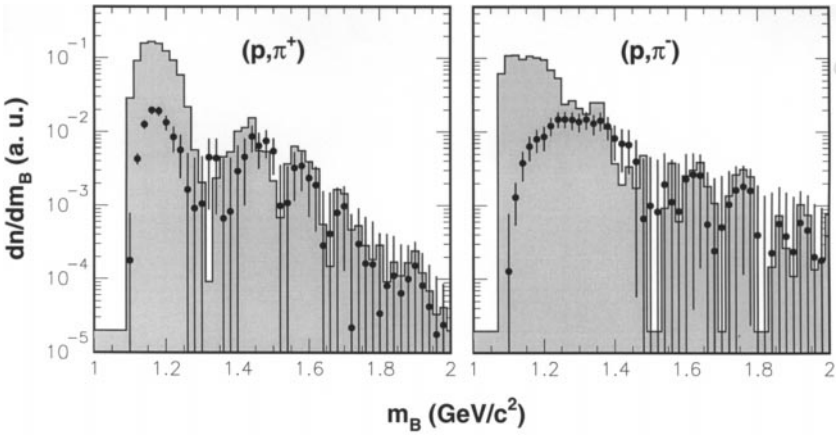

Fig. 6. The shaded areas show a logarithmic plot of the invariant mass spectra of correlated (p, π^+) (left panel) and (p, π^-) pairs (right panel) from the reaction Ni + Ni at 1.93 AGeV bombarding energy. The points display the equivalent spectra selecting pions with $p_t > 0.3$ GeV/c

Table 2. The first 2 rows of each reaction entry give the values of m_Δ and σ_Δ deduced from (p, π^+) respectively (p, π^-) pairs, the third row gives the same for the average $(p, \pi^\pm)$. The last row represents the results of the p_t analysis including, in addition to m_Δ and σ_Δ, also the fraction $r_{B>\Delta}$ of resonances with masses above the $\Delta(1232)$ resonance, and the relative fraction n_Δ of baryons excited to the $\Delta(1232)$ resonance

reaction	m_Δ (MeV/c^2)	σ_Δ (MeV/c^2)	$r_{B>\Delta}$	n_Δ (%)
Au + Au	1160 ± 10	38 ± 5		
at	1149 ± 10	48 ± 5		
1.06 AGeV	1154 ± 10	43 ± 5		
	1154 ± 5	48 ± 3	0.08 ± 0.03	6.5 ± 2
Ni + Ni	1173 ± 10	41 ± 5		
at	1171 ± 10	53 ± 5		
1.06 AGeV	1173 ± 10	47 ± 5		
	1175 ± 5	50 ± 3	0.10 ± 0.03	11.5 ± 3
Ni + Ni	1177 ± 10	41 ± 5		
at	1185 ± 10	56 ± 5		
1.45 AGeV	1181 ± 10	48 ± 5		
	1176 ± 5	51 ± 3	0.15 ± 0.05	16 ± 4
Ni + Ni	1174 ± 10	40 ± 5		
at	1166 ± 10	56 ± 5		
1.93 AGeV	1171 ± 10	48 ± 5		
	1182 ± 5	49 ± 3	0.21 ± 0.10	22 ± 6

are associated with the excitation of resonances above the $\Delta(1232)$ resonance. The defolding technique only proves that this conclusion is not in contradiction with the measured pion p_t spectra which could also contain thermal pions. The proof for the excitation of higher resonances requires that pions and protons from the decay of these resonances are correlated. In order to confirm that pions with large momenta are indeed emitted by these high resonances and that these pions are correlated with protons we have reanalyzed the $(p, \pi^\pm)$ data with a lower threshold of $p_t > 0.3$ GeV/c for the pion momentum. The invariant mass spectra, separated according to the pion charges, are shown in Fig. 6 for the Ni + Ni reaction at 1.93 AGeV incident energy. As shaded areas the Fig. 6 also displays the invariant mass spectra obtained without the threshold on the pion momenta. Two conclusions can be derived from Fig. 6:

- The tail of the mass distribution is strongly associated with high p_t pions, since the applied p_t cut reduces only the yield from the mass region $m_B < m_<$. This is, of course, required by the decay kinematics of the resonances, provided such resonances were excited.
- The shape of the deduced mass distribution is different for (p, π^+) and (p, π^-) pairs, and the number of correlated pairs has increased more for the π^- than the π^+. This asymmetry again confirms our earlier conclusions about the contribution of $I = 1/2$ resonances, since these cannot decay into (p, π^+) pairs.

5 Summary and discussion

In the present work we have shown that pions are produced in relativistic heavy ion reactions by the decay of excited baryon resonances, with the dominant contribution from the $\Delta(1232)$ resonance. The heavy ion reactions studied were Au + Au at 1.06 AGeV and Ni + Ni at 1.06, 1.45 and 1.93 AGeV incident energies. The mass distributions of the baryon resonances were deduced by means of two independent methods: Firstly by defolding the pion p_t spectra measured at midrapidity by means of (3), and secondly by calculating the invariant masses of correlated (p, π^+) respectively (p, π^-) pairs by means of (5). In both analyses the Coulomb distortions due to the nuclear matter distribution were compensated by adding the data obtained for π^+ and π^-. In case of the $(p, \pi^\pm)$ pairs this compensation was performed with the invariant mass spectra which were obtained separately for π^+ and π^-. The comparison between both suggests the additional excitation of $I = 1/2$ resonances, and it proves the persistence of the residual Coulomb distortion in the (p, π^-) respectively (p, π^+) correlations.

The results from both methods after the removal of the Coulomb distortions were shown in Fig. 4 and Table 2. The agreement between the mass distributions from the two independent methods is the prime indicator that systematic errors in our analysis are small. Relative to the mass of the

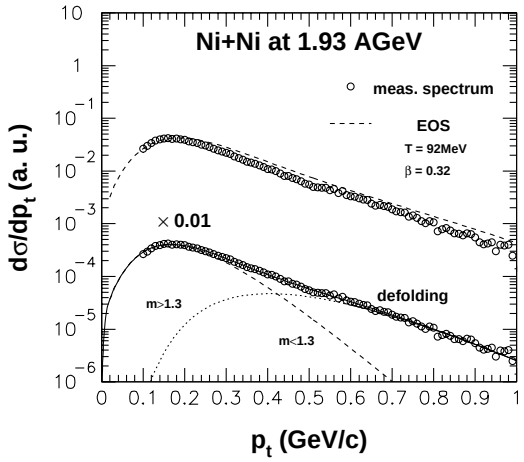

Fig. 7. Upper part: The p_t spectrum of $\pi^{\pm}$ measured(circles) and calculated(dotted curves) using the $f_{\Delta}(m_B)$ distribution of [19] and the T, β values published in [26]. Lower part: The decomposition of the p_t spectrum into the $\Delta(1232)$ component ($m_B < 1.3$) and the higher resonances component ($m_B > 1.3$)

free $\Delta(1232)$ resonance the maxima of the deduced mass distributions are shifted towards smaller masses. The mass shift is on the average $\Delta m_{\Delta} = -60 \pm 10$ MeV/c^2, where the lower limit corresponds to Au + Au, the upper limit to Ni + Ni near-central reactions. The width of the $\Delta(1232)$ remains almost unchanged. The mass shift is more than 2 times larger than found in the preliminary analysis of [20]. The main reason for the deviation is that $(p, \pi^{\pm})$ pairs with small relative angles between the particle momenta are not excluded in the present analysis as they were in [20], see also the discussion in the Appendix 6.2. Our analysis of the $(p, \pi^{\pm})$ pairs suggests that at least 50% of the detected pions are correlated with protons, i.e. they originate from the decay of baryon resonances. For the remaining part, the correlations are either destroyed by the residual scattering of the proton by nucleons, or those pions are of direct origin. The agreement between the mass spectra from the defolding and correlation analyses makes the former possibility more likely. In particular the application of p_t cuts in the correlation analysis indicates that firstly higher resonances then the $\Delta(1232)$ resonance are involved in the pion production, and that secondly at least part of these resonances have isospin $I = 1/2$.

The mass shift deduced presently and the almost unchanged width of the mass distribution are in close agreement with the recent results determined from (p, π^{+}) pairs in central Ni + Cu collisions at 1.97 AGeV bombarding energy in [19]. Nevertheless it should be pointed out that the resonance formula of [32] used in the analysis of [19] to describe the $\Delta(1232)$ mass distribution produces a tail which overestimates our measured p_t spectrum as demonstrated in the upper part of Fig. 7. Notice that the inclusion of even higher-lying resonances would only enhance the disagreement at large transverse momenta. We thus conclude that under the present conditions the mass distribution assigned to the dominant $\Delta(1232)$ resonance cannot be adequately described by the parametrization of [32].

There are two conceivable causes for these modifications of the resonance shape: The resonance masses are shifted because of their nuclear environment or/and the resonances are in thermal equilibrium with the hadronic matter at a low temperature.

The effect of the hadronic environment on the masses of hadrons was theoretically studied in many publications, for a recent review c.f. [33]. The environment causes in general a mass shift which can be either positive or negative and depends on the hadronic density. The verification of this prediction is at the moment of considerable interest, at *GSI* energies the experiments at present mainly focus on the kaon mass [34,35]. The situation with respect to baryons appears less understood. In a recent study [31] the mass of the $\Delta(1232)$ resonance was calculated to be shifted by $\Delta m_{\Delta} \approx -10$ MeV/c^2 when corrections due to the nucleon interaction in the πN loop of the Δ self energy are taken into account. The weight function $f_{\Delta}(m_B)$ which replaces in this calculation the free mass distribution of the $\Delta(1232)$ resonance is used in our further analysis.

On the other hand a hadronic environment at low temperature T and in thermal equilibrium with the baryon resonances will result in an apparent mass shift when these resonances decay. Of course, the hypothesis that all hadrons are in thermal equilibrium needs verification. But even if equilibrium is not established the development of nuclear radial flow will cause the resonances to be populated predominantly at the low-mass side in late stages of the reaction [8]. In the following we will assume for reasons of simplicity that the apparent mass shift of the $\Delta(1232)$ resonance can be described by a thermal weight function of Boltzmann type with temperature T_{Δ}. An estimate of T_{Δ}, which henceforth shall be called temperature although it should be considered primarily as fit parameter, is obtained by fitting the mass spectra in Fig. 4 by $f_{\Delta}(m_B) \cdot exp(-(m_B - m_0)/T_{\Delta})$ in the mass region $m_B < m_{<}$, where $f_{\Delta}(m_B)$ was taken from the calculations of [31]. The mass distributions obtained by both methods enter the fits with equal weights. The mass range 1150 MeV/c^2 $< m_B <$ 1250 MeV/c^2 is however considered with a larger statistical weight, since the very low masses $m_B <$ 1150 MeV/c^2 are expected to be stronger affected by the possible systematic errors of both analysis methods, and the larger masses $m_B >$ 1250 MeV/c^2 are stronger affected by the contribution from higher resonances. As an example the left panel of Fig. 8 displays the fit to the invariant mass distribution in case of the Ni + Ni reaction at 1.93 AGeV bombarding energy. The required temperature is in this case $T_{\Delta} = 59 \pm 8$ MeV, for the other reactions the temperatures are listed in Table 3. The errors represent the uncertainties of the fits deduced by slightly shifting the fit region. Notice that the deduced values of T_{Δ} depend on the used parametrization of the mass distribution. The parametrization of [32] leads to values for T_{Δ} smaller by approximately 30% than the ones listed in Table 3.

The temperatures T_{Δ} obtained in this way are of the order of 50 MeV and therefore much smaller than the temperatures deduced for the Au + Au and Ni + Ni reac-

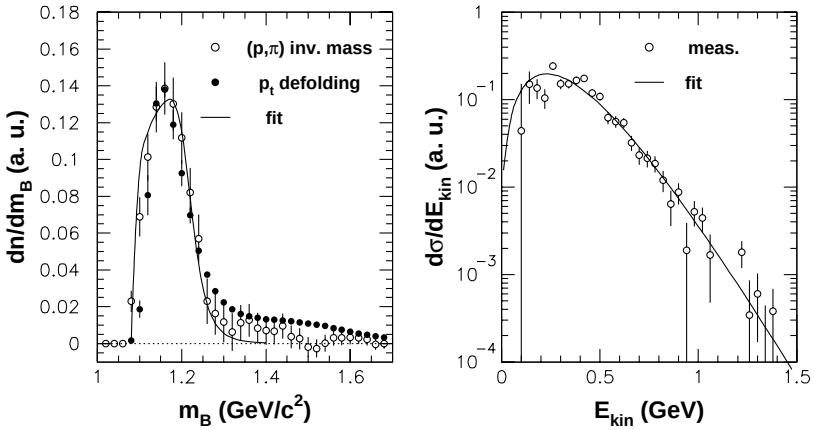

Fig. 8. Left panel: The measured (symbols) invariant mass spectrum of the Ni + Ni reaction at 1.93 AGeV bombarding energy, and the fit (curve) using the Boltzmann corrected $f_{\Delta}(m_{\rm B})$ distribution of [31]. Right panel: The kinetic energy spectrum (symbols) of the $\Delta(1232)$ resonances from the same reaction. The curve is a fit employing the Siemens-Rasmussen formula [25]. The values for the fitted temperature (left panel) and radial velocity (right panel) are listed in Table 3

Table 3. Temperatures T_{Δ} and radial flow velocities β_{Δ} deduced from a fit to the mass distributions in the range $m_{\rm B} < 1300$ MeV/c^2, and a fit to the kinetic energy distributions, c.f. Fig. 8. The first row is for the Au + Au reaction, the next three rows for the Ni + Ni reactions

energy(AGeV)	T_{Δ}(MeV)	β_{Δ}
1.06	41 ± 5	0.46 ± 0.03
1.06	53 ± 8	0.39 ± 0.05
1.45	60 ± 8	0.47 ± 0.04
1.93	59 ± 8	0.53 ± 0.04

tions by other means [22,26] and listed in Table 1. As pointed out earlier in [1], these small values of T_{Δ} are linked to the enhancement of the pion spectrum at very small transverse momenta, which cannot be explained by the mass distribution of the **free** $\Delta(1232)$ resonance, but requires the effective mass to be strongly shifted towards the threshold mass by a medium with low temperature.

We interprete the calculated mass distribution of Fig. 8 as the sole contribution from the $\Delta(1232)$ resonance, which for $m_{\rm B} = m_{<} = 1300$ MeV/c^2 practically has reached zero intensity. The remaining yield not accounted for is, because of its correlation with protons, at least partly caused by higher lying resonances. As pointed out before this interpretation is also suggested by the fact that the (p,π^-) and (p,π^+) invariant mass spectra are different for large pion momenta and that both pairs have different $\kappa_{\rm p}^{\pm}$ values, see Table 1. The upper estimate of the ratio between the contribution from high-lying resonances and the one from the $\Delta(1232)$ resonance is quoted in Table 2 as $r_{\rm B>\Delta}$. These values were extracted from the results of the defolding technique, since the analysis of the correlation results, also shown in Fig. 4, requires information about the admixtures of $I = 1/2$ and $I = 3/2$ states in the tails of the invariant mass distributions which does not exist with the required accuracy. We have used the latter results, however, to obtain the quoted errors of $r_{\rm B>\Delta}$. The contribution of the higher lying resonances to the $p_{\rm t}$ spectrum, obtained in this way, is shown in the lower part of Fig. 7. It demonstrates the difference to the alternative where the high-momentum tail is interpretated as mainly due to thermal pions: The distribution from thermal pions would continue to rise towards small $p_{\rm t}$ values and would give a thermal contribution which is larger than the values of $r_{\rm B>\Delta}$ quoted in Table 2, in agreement with [31].

With these informations and the known [1,2] dependence of the pion multiplicity on the number of participants $A_{\rm part}$, one may calculate the fraction n_{Δ} of participants which are excited to $\Delta(1232)$ resonances under the present experimental conditions. The values of n_{Δ} are listed in Table 2, they increase with bombarding energy primarily because the number of pions increases. Similar values for the fraction of $\Delta(1232)$ resonances populated in the Ni + Ni reactions were extracted in [26], where the high-momentum tail was interpreted as due to thermal pions emitted from an equilibrated radially expanding source with the temperatures T and the average expansion velocities β listed in Table 1.

According to the observed mass shifts in the current analysis the freeze out conditions for pions from late $\Delta(1232)$ decays would be characterized by a much lower value of $T_{\Delta} = 40 - 60$ MeV. This value when interpreted as temperature is of similar size as the average freeze out temperatures of protons in the complete phase space, extracted in recent analyses of the same present data samples [30,36] which also point to a larger collective energy and thus smaller temperatures than estimated from the kinetic energy spectra of pions and light charged particles alone. It is also in line with the analysis of the Au + Au reaction at lower bombarding energies [37].

On the other hand, the assumption of thermal equilibrium and instant freeze out at T_{Δ} fails to reproduce the $\Delta(1232)$ yield. As was shown in [26], where the attainment of equilibrium was postulated, the considerably higher temperatures listed in Table 1 are necessary to describe the observed production probabilities. These find-

ings are in agreement with [38] and are confirmed by an improved calculation where the widths of all higher-lying resonances were included via a Breit-Wigner parametrisation with parameters listed in the particle data booklet [39]. For a consistent treatment of the yields and the energy distributions of baryons and pions we drop the surface corrections and use the phase space density of infinite nuclear matter [10]. At a temperature of $T = 92$ MeV this model then predicts a value of approximately $r_{\mathrm{B}>\Delta} = 0.35$ for the ratio between higher-lying and the $\Delta(1232)$ resonance, in variance with the measured value given in Table 2. From the thermal model one may also deduce the contribution of thermal pions which increases with decreasing freeze out density. Estimating the upper limit of this contribution from the $\kappa_{\mathrm{p}}^{\pm}$ value of Table 1 and the published pion yield [1,2] the freeze out density ρ should be close to normal nuclear matter density ρ_0, whereas it is predicted that the majority of pions, i.e. those with small momenta, freeze out at $\rho \approx \rho_0/3$ [40,41].

These inconsistencies in the interpretation of the different experimental observations probably point to the fact that the simple picture of an instantaneous freeze out in thermal and chemical equilibrium is not justified. The number of baryon resonances and pions is determined very early in the reaction when the energy to excite these resonances is still sufficiently large [10]. The dominant part of the $\Delta(1232)$ resonances is measured at late stages of the reaction, when this energy has considerably decreased because of earlier π emissions, and because of the development of radial flow. In case one is allowed to interpret T_Δ as that part of the energy corresponding to unordered motion at freeze out one may deduce from resonances in the mass range $m_{\mathrm{B}} < m_<$ also the amount of energy converted into flow at the late stage of the reaction. We have reconstructed for those resonances their kinetic energy spectrum which is depicted in the right panel of Fig. 8 for the Ni + Ni reaction at 1.93 AGeV bombarding energy. The reconstruction procedure is equivalent to the one used to identify the resonances, i.e. the $E-m_{\mathrm{B}}$ spectrum of mixed pairs is subtracted from the one of measured pairs with a ratio $r^{\pm}$ which was determined earlier and is listed in Table 1. The kinetic energy spectra are corrected for the effects of the CDC geometry onto E and m_{B}. The resulting E_{kin} distribution of the shifted $\Delta(1232)$ resonance appears to have a maximum close to $E_{\mathrm{kin}} = 0.2$ GeV. The shape of this distribution suggests the existence of a strong collective flow. The fit by means of the Siemens - Rasmussen formula [25] with fixed mass $m_\Delta = 1180$ MeV/c^2 and temperature $T_\Delta = 59$ MeV and shown as full curve in the right panel of Fig. 8, yields a flow velocity $\beta_\Delta = 0.53 \pm 0.04$. The values of β_Δ deduced similarly from the other kinetic energy spectra of low-lying resonances are listed in Table 3. If interpreted in this way it shows that at late freeze out times of the pions the temperatures do not change significantly in the Ni + Ni systems, but the radial flow velocities increase with energy. The Au + Au system, compared with the Ni + Ni system, is characterized by a lower temperature and larger radial flow velocity.

Table 4. The values of the mass m_Δ and the width σ_Δ obtained from π^0, π^-, π^+, and the average $\pi^\pm$ by the analysis of (p,π) pairs or by the defolding technique

	pair analysis		defolding	
	m_Δ (MeV/c^2)	σ_Δ (MeV/c^2)	m_Δ (MeV/c^2)	σ_Δ (MeV/c^2)
π^0	1201 ± 3	51 ± 2	1198 ± 2	48 ± 1
π^-	1197 ± 3	50 ± 2	1180 ± 3	56 ± 2
π^+	1207 ± 3	49 ± 2	1228 ± 2	34 ± 2
$\pi^\pm$	1202 ± 2	50 ± 2	1202 ± 2	51 ± 2

Because of the very low nuclear temperatures deduced from our analysis one cannot neglect the possibility that the shifts of the resonance mass might be induced by still other effects of the nuclear environment than those already considered in [31]. In [33] the alternatives are discussed in some detail. In case the mass shift scales with the nuclear density and higher lying resonances are excited more abundantly in the earlier times of large densities the observed mass spectrum of the baryon resonances would be rather complex and difficult to decompose in contributions from specific resonances. From Fig. 6 it appears that whatever the true mechanism is, it produces a resonance mass distribution with near-exponential decline towards larger mass values. It was indeed this exponential decline which was used very early by Chapline et al. [42] to study the properties of dense hadronic matter.

6 Appendix

6.1 Effects due to the Coulomb interaction

The Coulomb residual interaction between the nuclear matter distribution and charged mesons modifies the primordial phase space distributions of the latter after they were emitted by resonance decays. The size of this modification is particularly strong for pions because of their small mass, and it is readily observed in experiments: The momentum distribution of positive and negative pions differ for small momenta, the difference is still observed in systems with total charge $Z < 60$ [2]. In a recent theoretical paper based on BUU calculations [40], it was proposed that the π^-/π^+ difference provides a sensitive method to investigate the nuclear matter distribution at SIS energies.

In our Monte Carlo studies of how the Coulomb effects may change the deduced mass distributions of baryon resonances we have employed a slightly simpler model which is based on a spherical and radially expanding baryon distribution in thermal equilibrium. The $\Delta(1232)$ resonances with the mass distribution $f_\Delta(m_{\mathrm{B}})$ are present in the baryon distribution with fraction n_Δ, they can decay via π^+, π^-, or π^0 emission only at the surface of this distribution. After the decay the emitted particles are propagated in the Coulomb field of the baryon distribution. The positions and the momenta are calculated in relativistic kinematics, the time steps are sufficiently small to

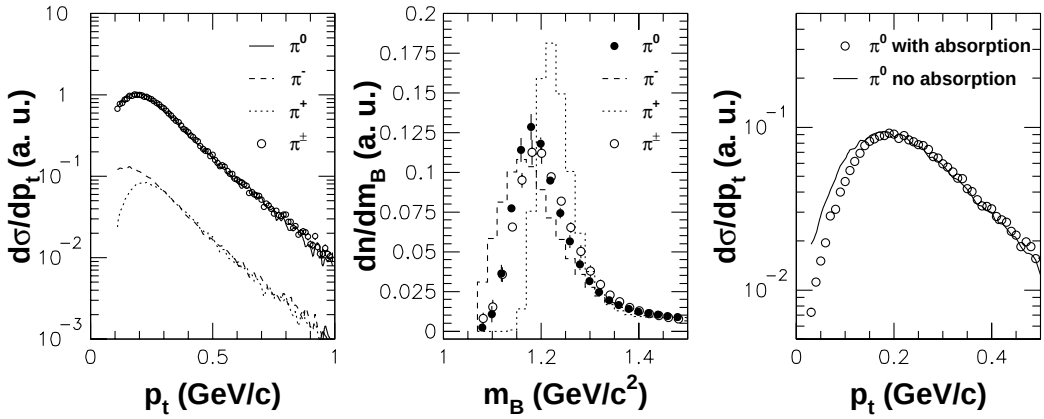

Fig. 9. The left panel displays the calculated p_t distributions of π^0, π^-, and π^+ (curves). The circles present the sum of the π^- and π^+ distributions. The centre panel displays the invariant mass distributions obtained by defolding the p_t spectra of the left panel. The right panel illustrates the reduction of low-momentum π^0 caused by their absorption in the source

handle the complete momentum range of pions. The final momentum is reached, when the relative change of the momentum becomes smaller than 10^{-6}. In case the total energy approaches the pion rest mass, this is only possible for π^- because of their negative Coulomb potential, the particle is considered to be in a bound state and cannot be detected. Furthermore we use an absorption probability of 0.2 for those pions, which revert into the baryon distribution. Notice that absorption can occur for all pion charges, the probability depends on the relation between the momentum of the decaying resonance and the momentum of the pion emitted by the decay. To be close to the situation of the Au + Au reaction we consider a source of normal nuclear matter density with 310 baryons and a total charge given by the N/Z ratio of Au [41]. The kinetic energy of the baryons is assumed to be distributed according to the formula of Siemens and Rasmussen [25] with a temperature $T = 81$ MeV and an expansion velocity $\beta = 0.32$. In addition to the geometrical and the detection limits of the CDC we also include the finite momentum resolutions of the CDC, characterized by the parameters $\sigma(p_t)/p_t = 0.05$, $\sigma(\varphi) = 1°$, and $\sigma(\vartheta) = 5°$ [1].

This simple model is sufficient to reproduce the gross features of the measured [1,2] transverse momentum spectra of $\pi^{\pm}$, i.e. their difference at momenta $p_t < 0.3$ GeV/c, and their identical decline for higher transverse momenta, see Fig. 9 left panel. It is also evident that the sum of the π^+ and π^- momentum distributions is a good approximation for the primordial momentum distribution obtained from π^0. It is therefore not surprising that the primordial $\Delta(1232)$ mass distribution $f_\Delta(m_B)$ is not retrieved from the distorted pion momenta. The defolding of the pion p_t spectra yields from the π^- respectively π^+ a $f_\Delta(m_B)$ distribution which is shifted to smaller/larger masses, see Fig. 9 centre panel, whereas the sum of both p_t spectra allows to obtain with good approximation the undistorted $f_\Delta(m_B)$ distribution as expected since the Coulomb effects cancel when the p_t spectra of π^- and π^+ are added.

It might be interesting to illustrate how the pion absorption in nuclear matter changes the pion p_t distributions. In Fig. 9 right panel the p_t spectra of π^0 are compared with and without absorption. It is obvious that absorption mainly suppresses pions with small transverse momenta. On the other hand this part of the momentum distribution becomes enhanced again when the decay channel into 2π opens. Therefore the net effect is presumably small, and it is beyond the scope of the present study to disentangle these effects experimentally.

The situation becomes more complicated when looking at the correlations between pions and protons. In Fig. 1 we have shown how the geometric boundaries of the CDC reduce the detection efficiency for small resonance masses. In the left panel of Fig. 10 the uncorrected invariant mass spectrum from (p, π^0) pairs is plotted which shows the size of this effect. On the other hand, when the finite detector resolutions are considered one finds an enhancement of the invariant mass distribution at small masses. Including both effects one obtains in our Monte Carlo simulations an invariant mass distribution very close to the input. The cancellation of different effects is not always observed. In case of the energy distribution of resonances we find in the right panel of Fig. 10 that these are mainly effected by the geometric boundaries, and that corrections have to be applied to restore the original distribution from the measurement. The corrections are considered reliable only for kinetic energies $E_{\rm kin} > 100$ MeV.

The effects of the residual Coulomb interaction on the invariant masses from $(p, \pi^{\pm})$ pairs are shown in Fig. 11. Qualitatively the situation is similar to the analysis of the p_t spectra shown in Fig. 9. The $f_\Delta(m_B)$ distribution deduced from the (p, π^-) respectively (p, π^+) pairs are also shifted to smaller/larger masses relative to the mass distribution from correlated (p, π^0) pairs. On the other hand the average mass distribution from both (p, π^-) and (p, π^+) pairs comes very close to the undistorted distribution.

The sizes of the mass shifts m_Δ and the widths σ_Δ deduced from our Monte Carlo studies are listed in Table 4. It is evident that the results from the correlation analyses are less affected by the Coulomb distortion than those from the defolding analysis. Nevertheless adding the

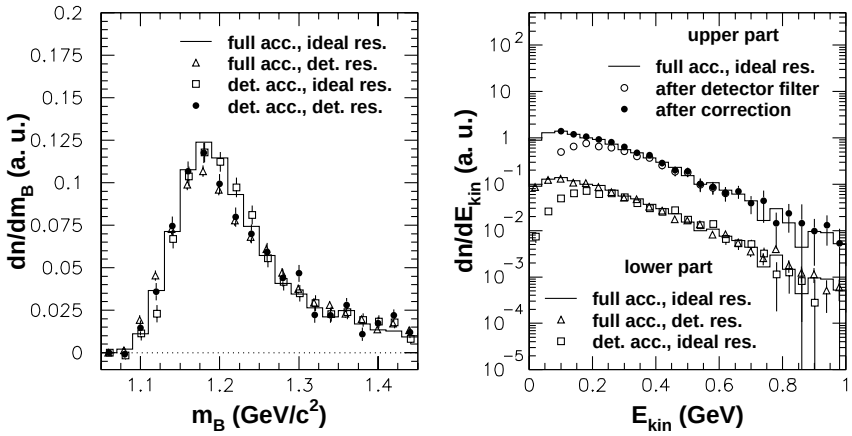

Fig. 10. The influences of finite detector acceptance and resolution on the resonance mass (left panel) and kinetic energy (right panel) distributions deduced from correlated (p, π^0) pairs

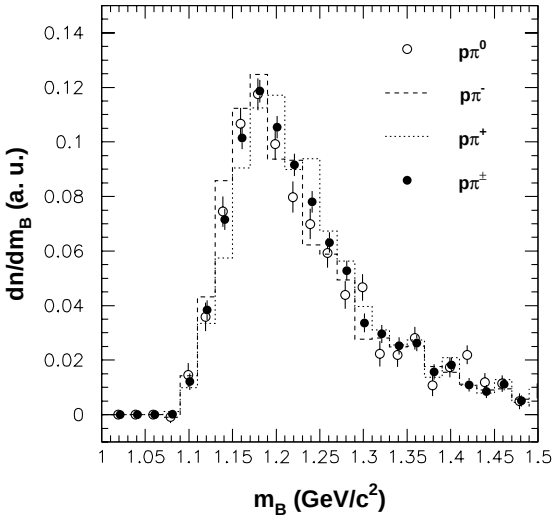

Fig. 11. Comparison between the resonance mass distributions from $(p\pi^0)$, $(p\pi^-)$, and $(p\pi^+)$ pairs. The $(p\pi^\pm)$ distribution corresponds to the normalized sum of the $(p\pi^-)$ and $(p\pi^+)$ distributions

π^- and π^+ data one comes closest to the primordial conditions, which is the procedure employed in the present analysis.

6.2 Effects due to the tracking efficiency

The discussion in Sect. 2 is primarily concerned with the efficiency of reconstructing the baryon resonances within the geometrical boundaries of the *CDC*. Another efficiency reduction, which requires a careful investigation, is imposed by the limited capabilities of the available tracking algorithms to separate and identify individual particle tracks in the *CDC*. These inefficiencies become largest when the mass of the decaying resonance is close to the threshold mass m_0, i.e. when the relative momentum between the proton and the pion is small and the two particle tracks are close to each other. For the tracking algorithm, which analyzes particle tracks in the xy plane perpendicular to the z direction of the magnetic field, the closeness of tracks is given by the relative angle $\alpha_\mathrm{t} = \varphi^{(\pi)} - \varphi^{(\mathrm{p})}$ and by the magnitude of $p_\mathrm{t}^{(\pi)}$. The smaller α_t and the larger $p_\mathrm{t}^{(\pi)}$ the more difficult it becomes to separate pion tracks from proton tracks.

The size of the efficiency reduction as function of α_t and $p_\mathrm{t}^{(\pi)}$ can be obtained from a comparison of the invariant mass distributions $\frac{dn(meas)}{dm_\mathrm{B}}$ and $\frac{dn(mixed)}{dm_\mathrm{B}}$ as functions of α_t and $p_\mathrm{t}^{(\pi)}$ since in the latter all pairs are identified with identical efficiencies. We show in Fig. 12 the ratio $\omega = \frac{dn(meas)}{dn(mixed)}$ for (p, π^-), (p, π^+), and Monte Carlo generated (p, π) tracks as functions of α_t, where the Monte Carlo simulation illustrates the ideal case of complete tracking efficiency. In the simulation the conditions are similar to the experimental ones, in particular the fraction of $(p, \pi^\pm)$ pairs due to resonance decay is in the order of 1%. The comparison with the Monte Carlo simulation proves, that the probability to miss correlated $(p, \pi^\pm)$ pairs never exceeds 20% for a given value of α_t, and that it is certainly more appropriate to correct for this inefficiency than to remove all data with $|\alpha_\mathrm{t}| < 50°$, as was done in [20].

That the efficiency reduction is different for (p, π^-) and (p, π^+) pairs was to be expected since the p and π^+ have the same curvature signs, whereas these are different in case of p and π^-. Furthermore the fact that in case of (p, π^-) pairs the efficiency is reduced only for negative α_t angles offers the possibility to check the consistency of the efficiency correction. The invariant mass spectra $\frac{dn}{dm_\mathrm{B}}$ have to be the same for $\alpha_\mathrm{t} < 0$ and $\alpha_\mathrm{t} > 0$. This check was done in our analyses and was shown to yield identical $\frac{dn}{dm_\mathrm{B}}$ distributions within the given uncertainties. All data shown in this paper were therefore efficiency corrected according to the results of Fig. 12 and the similar dependences on $p_\mathrm{t}^{(\pi)}$. The sizes of the efficiency corrections were directly obtained from the data, their dependence on α_t and $p_\mathrm{t}^{(\pi)}$ was, however, smoothed by the spline algorithm.

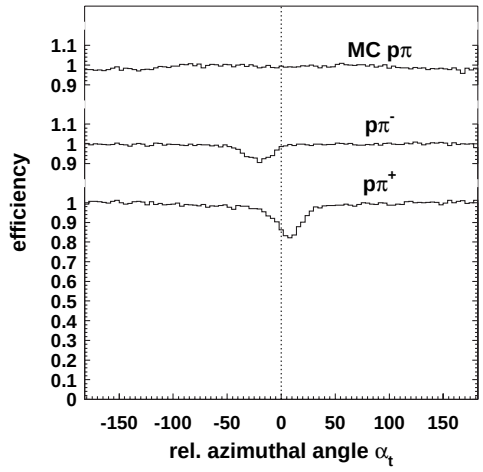

Fig. 12. Efficiency to identify a proton and a pion track as function of the relative angle $\alpha_{\rm t}$ between these two tracks in the x, y plane perpendicular to the magnetic field

We would like to thank W. Weinhold for providing us with his $f_\Delta(m_{\rm B})$ function. This work was supported in part by the Bundesministerium für Forschung und Technologie under contract 06 HD 525 I(3) and by the Gesellschaft für Schwerionenforschung under contract HD Pel K and by the Korea Research Foundation under contract 1997-001-D00117.

References

1. **FOPI** collaboration: D. Pelte et al., Z. Phys. A. **357**, 215 (1997)
2. **FOPI** collaboration: D. Pelte et al., Z. Phys. A. **359**, 55 (1997)
3. G.F. Bertsch, S. Das Gupta, Phys. Rep. **160**, 189 (1988)
4. W. Cassing, K. Niita, S.J. Wang, Z. Phys. A **331**, 439 (1988)
5. W. Cassing, V. Metag, U. Mosel, K. Niita, Phys. Rep. **188**, 363 (1990)
6. J. Aichelin, Phys. Rep. **202**, 233 (1991)
7. S.A. Bass GSI-93-13 Report (1993)
8. S.A. Bass, C. Hartnack, H. Stöcker, W. Greiner, Phys. Rev. C **50**, 2167 (1994)
9. S.A. Bass, C. Hartnack, H. Stöcker, W. Greiner, Phys. Rev. C **51**, 3343 (1995)
10. P. Danielewicz, Phys. Rev C **51**, 716 (1995)
11. S. Teis, W. Cassing, M. Effenberger, A. Hombach, U. Mosel, G. Wolf, Z. Phys. A. **356**, 421 (1997)
12. R. Brockmann, J.W. Harris, A. Sandoval, R. Stock, H.Stroebele, G. Odyniec, H.G. Pugh, L.S. Schroeder, R.E. Renfordt, D. Schall, D. Bangert, W. Rauch, K.L. Wolf, Phys. Rev. Lett. **53**, 2012 (1984)
13. A. Sandoval, R. Brockmann, R. Stock, H.Stroebele, D. Bangert, W. Rauch, R.E. Renfordt, D. Schall, J.W. Harris, G. Odyniec, H.G. Pugh, K.L. Wolf, GSI-85-10 Report (1985)
14. P. Senger, in: Multiparticle Correlations and Nuclear Reactions, ed. by J. Aichelin and D. Ardouin (World Scientific Publ. Co., 1994), page 285
15. **E814** collaboration: J. Barrette et al., Phys. Lett. B **351**, 93 (1995)
16. **DIOGENE** collaboration: M. Trzaska et al., Z. Phys. A **340**, 325 (1991)
17. J. Chiba, T. Kobayashi, T. Nadae, I. Arai, N. Kato, H. Katayama, A. Manabe, M. Tanaka, K. Tomizawa, D. Beatty, G. Edwards, C. Glashauser, G.J. Kumartzki, R.D. Ransome, T.T. Baker, Phys. Rev. Lett. **67**, 1982 (1991)
18. T. Hennino, B. Ramstein, D. Bachalier. H.G. Bohlen, J.L. Boyard, C. Ellegaard, C. Gaarde, J. Gosset, J.C. Jourdain, J.S. Larsen, M.C. Lemaire, D.L. Hote, H.P. Morsch, M. Österlund, J. Poitou, P. Radvanyi, M. Roy-Stephan, T. Sams, K. Sneppen, O. Valette, P. Zupranski, Phys. Lett. B **283**, 42 (1992)
19. **EOS** collaboration: E.L. Hjort et al., Phys. Rev. Lett. **79**, 4345 (1997)
20. M. Trzaska, in: Multiparticle Correlations and Nuclear Reactions, ed. by J. Aichelin and D. Ardouin (World Scientific Publ. Co., 1994), page 95
21. **TAPS** collaboration: F.-D. Berg et al., Phys. Rev. Lett. **72**, 977 (1994)
22. **EOS** collaboration: M.A. Lisa et al., Phys. Rev. Lett. **75**, 2662 (1995)
23. **KaoS** collaboration: C. Müntz et al., Z. Phys. A **357**, 1399 (1997)
24. J. Sollfrank, P. Koch, U. Heinz, Z. Phys. C **52**, 593 (1991)
25. P.J. Siemens, J.O. Rasmussen, Phys. Rev. Lett. **42**, 880 (1979)
26. **FOPI** collaboration: N. Herrmann et al., Nucl. Phys. **A610**, 49c (1996); B. Hong, et al., Phys. Lett. B **407**, 115 (1997); B. Hong et al., Phys. Rev. C **57**, 244 (1998)
27. A.P. Dempster, N.M. Laird, D.B. Rubin, J. Roy. Stat. Soc. B **39**, 1 (1977)
28. H. Durst, Staatsexamensarbeit (Faculty of Mathematic, University of Heidelberg (1995)), unpublished
29. D. L'Hôte, Nucl. Instr. Meth. **A337**, 544 (1994)
30. **FOPI** collaboration: M. Korolija et al., to be published
31. W. Weinhold, B.L. Friman, W. Nörenberg, Acta Phys. Pol. B **27**, 3249 (1996)
32. J. Cugnon, M.C. Lemaire, Nucl. Phys. **A489**, 781 (1988)
33. C.M. Ko, G.Q. Li, J. Phys. G **22**, 1673 (1996)
34. **KaoS** collaboration: R. Barth et al., Phys. Rev. Lett. **78**, 4007 (1997)
35. **FOPI** collaboration: J. Ritman et al., Z. Phys. A **352**, 355 (1995)
36. **FOPI** collaboration: R. Kotte et al., Z. Phys. A **359**, 47 (1997)
37. **FOPI** collaboration: W. Reisdorf et al., Nucl. Phys. **A612**, 493 (1997)
38. R. Averbeck et al., nucl-ex/9803001, to be published
39. Rev. of Part. Prop., Phys. Lett. Phys. Lett. B **239** (1990)
40. S. Teis, W. Cassing, M. Effenberger, A. Hombach, U. Mosel, G. Wolf, Z. Phys. A **359**, 297 (1997)
41. V.S. Uma Maheswari, C. Fuchs, A. Faessler, L. Sehn, D.S. Kosov, Z. Wang, nucl-th/9706004, to be published in Nucl. Phys. **A**
42. G.F. Chapline, M.H. Johnson, E. Teller, M.S.Weiss, Phys. Rev. D **8**, 4302 (1973)